fire

MDPI

Article

Forest Fire-Damaged Area Boundary Delineation Using a Hierarchical Ensemble U-Net with Sentinel-2 Imagery

Geonhwi Jung [1], Seunghyun Hong [2], Mooyoung Lim [1], Nahyun Park [1], Bomok Choi [1], Choongshik Woo [3], Yongku Kim [2], Bomi Kim [4] and Joowon Park [5,*]

[1] Department of Forestry, Kyungpook National University, Daegu 41566, Republic of Korea; alzaki3050@knu.ac.kr (G.J.); m01888@knu.ac.kr (M.L.); parknah123@knu.ac.kr (N.P.); bm4227@knu.ac.kr (B.C.)
[2] Department of Statistics, Kyungpook National University, Daegu 41566, Republic of Korea; edwin30@knu.ac.kr (S.H.); kim.1252@knu.ac.kr (Y.K.)
[3] Landslide Division, National Institute of Forest Science, Seoul 02455, Republic of Korea; woocs@korea.kr
[4] Forest Ecosystem Restoration Division, Korea Forest Service, Daejeon 35208, Republic of Korea; bm0901@korea.kr
[5] School of Forest Science and Landscape Architecture, Kyungpook National University, Daegu 41566, Republic of Korea
* Correspondence: joowon72@knu.ac.kr

Abstract

Climate change has prolonged droughts and intensified heatwaves worldwide, increasing the frequency, intensity, and spatial extent of forest fires. In South Korea, an increasing incidence of large forest fires has created a need for rapid, accurate forest fire-damaged area boundary delineation to support post-fire recovery and restoration planning. This is particularly important in South Korea, where the forest-fire season is followed by the summer rainy season, increasing the risk of post-fire soil erosion and slope instability and thereby increasing the need for rapid stabilization and restoration measures. However, previous studies have reported varying delineation performance depending on the input configuration, suggesting the need to examine how different spectral inputs and their integration affect boundary delineation. To address this limitation, we propose a hierarchical ensemble U-Net framework for forest fire-damaged area boundary delineation using Sentinel-2 imagery. To design the input data structure, differences between burned and unburned areas were examined using the Blue, Green, Red, RedEdge, and NIR bands and the NDVI and dNDVI indices, and four three-channel combinations (Blue–Green–Red, Blue–Green–RedEdge, Green–Red–NIR, and Green–RedEdge–NIR) and two single indices (NDVI and dNDVI) were chosen as inputs. Three U-Net models were then evaluated: a single-channel dNDVI model, a three-channel NIR-RE-G model, and a hierarchical ensemble model, which integrated the outputs of six independently trained U-Nets. Among the three models, the single-channel dNDVI model showed higher overall accuracy (84.1%), producer's accuracy (89.0%), and F1-score (0.80) than the three-channel NIR-RE-G model (82.9%, 70.7%, and 0.77, respectively), whereas the NIR-RE-G model achieved higher user accuracy (91.8%); the hierarchical ensemble model yielded the best overall performance, with the highest overall accuracy (85.7%), producer's accuracy (92.2%), and F1-score (0.83). This suggests that integrating complementary spectral responses can mitigate the limitations of single-input models and support more robust boundary delineation across the six tested wildfire cases in South Korea.

Keywords: forest fire; burned-area boundary delineation; satellite imagery; deep-learning; U-net; hierarchical ensemble model

Check for updates

Academic Editors: Grant Williamson, Nicholas LaHaye, Olga Kalashnikova and Huikyo Lee

Received: 6 August 2026
Revised: 25 October 2026
Accepted: 4 November 2026
Published: 9 November 2026

Copyright: © 2026 by the authors. Licensee MDPI, Basel, Switzerland. This article is an open access article distributed under the terms and conditions of the Creative Commons Attribution (CC BY) license.

1. Introduction

As climate change has intensified, in recent years, prolonged droughts and high-temperature conditions have increased the frequency, intensity, and affected area of forest fires worldwide, seriously threatening ecosystem stability and public safety [1–3]. With more extensive forest fire damage, delayed ecosystem recovery and response can aggravate secondary impacts, such as reduced ecosystem resilience, accelerated soil erosion, water pollution, and landslides [4–6]. In South Korea, where forests occupy approximately 63% of the national land area, accurate and timely forest-fire monitoring is particularly important because fires can affect extensive mountainous forest areas and the forest-fire season is typically followed by the summer rainy season. This increases the need for rapid post-fire recovery and restoration planning, slope stabilization, sanitary cuttings, and the mitigation of secondary damage such as soil erosion and landslides in burned mountainous areas. Accordingly, timely recovery and response require not only rapid identification of burned areas but also precise delineation of their boundaries [7,8]. To accurately identify damage extent, it is necessary to go beyond simple burned area detection, which merely determines whether an area has been affected by forest fire, and to perform burned area boundary delineation, which precisely defines the spatial boundary between burned and unburned areas. In South Korea, the rugged terrain and the prevalence of mixed coniferous–deciduous stands give rise to highly heterogeneous damage patterns, making precise boundary delineation especially important. If boundary delineation is inaccurate, errors may occur in the selection of restoration target areas, resulting in unnecessary sanitary cuttings in lightly damaged areas or the omission of severely damaged areas from restoration, delaying ecological recovery [9]. Furthermore, omission and commission errors in damaged-area mapping may distort restoration priorities and lead to inefficient resource allocation, ultimately increasing overall restoration costs [10,11].

In the past, forest fire-damaged area boundary delineation relied primarily on field surveys. However, for large forest fire-damaged areas, the extent of the damage and restricted site accessibility increase the time and cost of field surveys, limiting their effectiveness. Accordingly, satellite imagery, which enables repeated observation over a broad area, has become a major data source for forest fire damage detection [12–15]. In research, satellite imagery has been applied to forest fire-damaged area boundary delineation using a wide variety of approaches, ranging from global-scale monitoring using low-resolution sensors, such as MODIS, to detailed boundary delineation using medium-resolution satellite imagery, such as Landsat and Sentinel-2 [13,16–19]. Sentinel-2 data is considered suitable for detailed boundary delineation because it includes RedEdge and near-infrared (NIR) bands, which are useful for forest fire-damaged area detection, and can acquire images rapidly due to its 5-day revisit cycle [12,13,19,20].

More recently, satellite image-based forest fire-damaged area boundary delineation methods have evolved from index-based rule approaches to machine-learning and deep-learning-based image classification approaches [21]. Early studies detected damaged-area boundaries by applying fixed thresholds to single-date indices, such as the normalized difference vegetation index (NDVI) and normalized burn ratio (NBR). Subsequently, indices based on pre- and post-fire differences, e.g., the differenced NDVI (dNDVI) and differenced normalized burn ratio (dNBR), were used to reduce the false detection of non-vegetated areas as burned areas and incorporate the degree of change caused by the event into damage assessment [22–26]. However, although computationally simple, index-based rule approaches have inherent limitations. The accuracy of detection is inconsistent when the same threshold is applied at different acquisition times or seasons and under different soil conditions, as spectral reflectance varies according to these factors. In addition, boundary errors may increase because of mixed pixels and terrain shadow effects [27]. To address such

limitations, machine-learning (ML) approaches were introduced. Initially, unsupervised classification methods based on, for example, the ISODATA or K-means algorithms were applied; however, these were limited by subjectivity in the interpretation of results because the classifications vary depending on the number of clusters and initialization settings, and the analyst had to determine which clusters corresponded to damaged areas [20,28,29]. To overcome this limitation, supervised classification algorithms, such as random forest (RF), support vector machine (SVM), and classification and regression trees (CART), were applied. When trained on labeled burned and unburned area data, these methods enabled more objective classification and tended to improve detection accuracy under certain conditions [30–32]. However, ML methods are highly dependent on the training data, and their generalizability may be limited when the training data are biased toward specific regions and/or time periods [10,14,30]. In addition, since these methods process spectral values independently at the pixel level, spatial contextual information between adjacent pixels is difficult to incorporate into learning, representing an inherent structural limitation. On the other hand, deep-learning (DL)-based image segmentation methods can simultaneously incorporate spatial correlations and spectral information, and such methods have been applied to forest fire-damaged area boundary delineation [33–39]. Deep learning reduces the need for analysts to manually select training samples, and by automatically learning complex nonlinear features and spatial patterns, it enables more generalized feature extraction than conventional machine learning [10,40]. In particular, the U-Net architecture extracts relatively precise boundary information in forest fire-damaged areas with diverse spectral characteristics because of its encoder–decoder structure and use of skip connections, which effectively combine multi-scale features [41–43].

Previous studies have shown that U-Net-based burned-area mapping performance can vary according to the selected input variables, model type, and setting in South Korea [34,37]. However, fewer studies have examined whether predictions derived from multiple spectral configurations can be hierarchically integrated for forest fire-damaged boundary delineation in complex mountainous environments. Forest fire-damaged areas contain heterogeneous spectral and spatial characteristics, which depend on damage type, with crown fires, heat injury, and surface fires creating distinct signatures. This is particularly evident in South Korea, where the rugged topography and complex stand composition produce pronounced variations in burn severity. Consequently, the resulting spatial and spectral heterogeneity of damaged areas calls for more detailed boundary delineation than has been achieved in previous studies. However, when such areas are analyzed using a single-layer input structure, sensitivity bias toward spectral responses may occur, or interference among different spectral characteristics may arise, resulting in the over- or under-delineation of damage-area boundaries [27,44–46]. Thus, although deep learning has overcome the structural limitations of machine learning, it is still limited by input-data design and does not sufficiently incorporate the spectral diversity of forest fire-damaged areas [42,47,48]. Furthermore, whereas a specific input combination or single model may perform effectively in a given region, its generalization capability is often limited when transferred to regions with differing conditions or to areas of mixed burn severity. Accordingly, to adequately account for diverse environmental conditions and damage characteristics, the predictions of multiple models trained on distinct spectral combinations and vegetation indices must be jointly considered. Notably, ensemble learning can reduce bias and variance and improve generalizability by integrating the predictions of multiple models [45].

In this study, we constructed a hierarchical ensemble U-Net model in which models were independently trained on different spectral combinations and vegetation-index input data, and the predictions of the individual models were reconfigured into a new multi-channel input dataset for a second round of segmentation. Through this approach, we

aimed not only to compare alternative spectral input configurations, but also to examine whether predictions derived from multiple spectral representations could be hierarchically integrated for boundary delineation and whether a model trained on external fire-perimeter data could be applied to independently prepared wildfire cases in South Korea.

2. Materials and Methods

2.1. Study Sites

This study was conducted on six large areas in South Korea affected by forest fires that occurred between April 2020 and June 2022 (Figure 1, Table 1). The study sites were in Andong-si, Bonghwa-gun, Gunwi-gun, Ulgin-gun, Miryang-si and Yanggu-gun. The dates of occurrence, including the fire start and suppression dates, and the area damaged for each forest fire are listed in Table 1. The damaged area ranged from a minimum of 137 ha (Bonghwa, April 2022) to a maximum of 1931 ha (Andong, April 2020), and most events occurred during the spring season, from April to May. During this period, forest fires spread very rapidly because of hot and dry climatic conditions and strong slope winds. All six study sites were characterized by conifer-dominated forests, with *Pinus densiflora* as the dominant tree species.

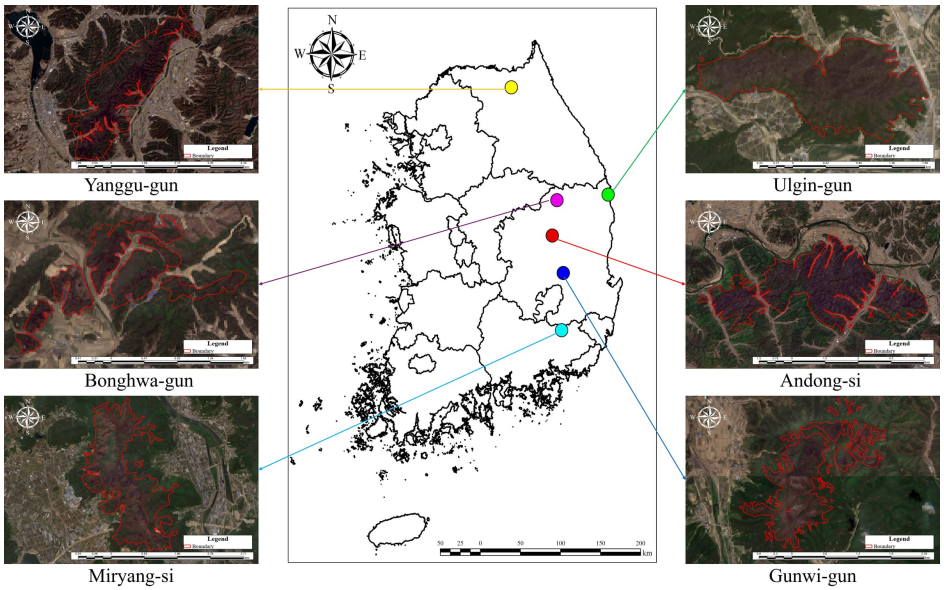

Figure 1. Study sites in South Korea.

Table 1. Overview of the study sites, including forest fire occurrence dates and the areas damaged.

Study Site	Dominant Forest Type	Dominant Species	Fire Start Date	Fire Suppression Date	Damaged Area (ha)
Andong	Conifer	*Pinus densiflora*	24 April 2020	26 April 2020	1931
Bonghwa			5 April 2022	6 April 2022	135
Gunwi			10 April 2022	12 April 2022	214
Yanggu			10 April 2022	12 April 2022	719
Ulgin			28 May 2022	29 May 2022	231
Miryang			31 May 2022	6 June 2022	571

2.2. Data

2.2.1. Training Data

The training data used in this study were obtained from a forest fire-damaged area dataset provided by Wildland Fire Interagency Geospatial Services (WFIGS), which is

operated by the USDA Forest Service and the National Interagency Fire Center (NIFC) [49]. For valid "Wildfire," and "Prescribed Fire," events registered in the Integrated Reporting of Wildland Fire Information (IRWIN) system, WFIGS provides damage boundaries. In this study, forest fires with damaged areas of 100 ha or more occurring after January 2018 were selected from the WFIGS dataset, and polygons representing the damage boundaries of each event were extracted and used as training data.

WFIGS fire perimeters were used in this study as training labels for learning fire-affected boundary patterns. Because these data represent operational fire perimeters rather than exact pixel-level burned-area masks, some polygons may include unburned areas within the delineated perimeter. Accordingly, the WFIGS dataset was used as a fire-damaged area label source for model training rather than as a direct reference mask for final accuracy assessment.

After applying the selection criteria, the final training dataset consisted of 2020 fire events, including 1914 wildfires and 106 prescribed fires. Since the purpose of this study was to delineate fire-damaged area boundaries rather than to classify fire types, the two event types were used together as a single fire-affected training dataset. The selected fire events were distributed across multiple geographic regions within the WFIGS domain, thereby providing training samples under diverse environmental conditions (Figures 2 and 3). To construct the model-development dataset, 90% of the WFIGS events were assigned to the training set and the remaining 10% were used as the validation set. For the hierarchical ensemble model, however, a fold-based procedure was additionally used when generating the first-stage probability maps for second-stage training, so that the second-stage input was constructed from held-out first-stage predictions rather than from the same samples used to fit the corresponding first-stage models.

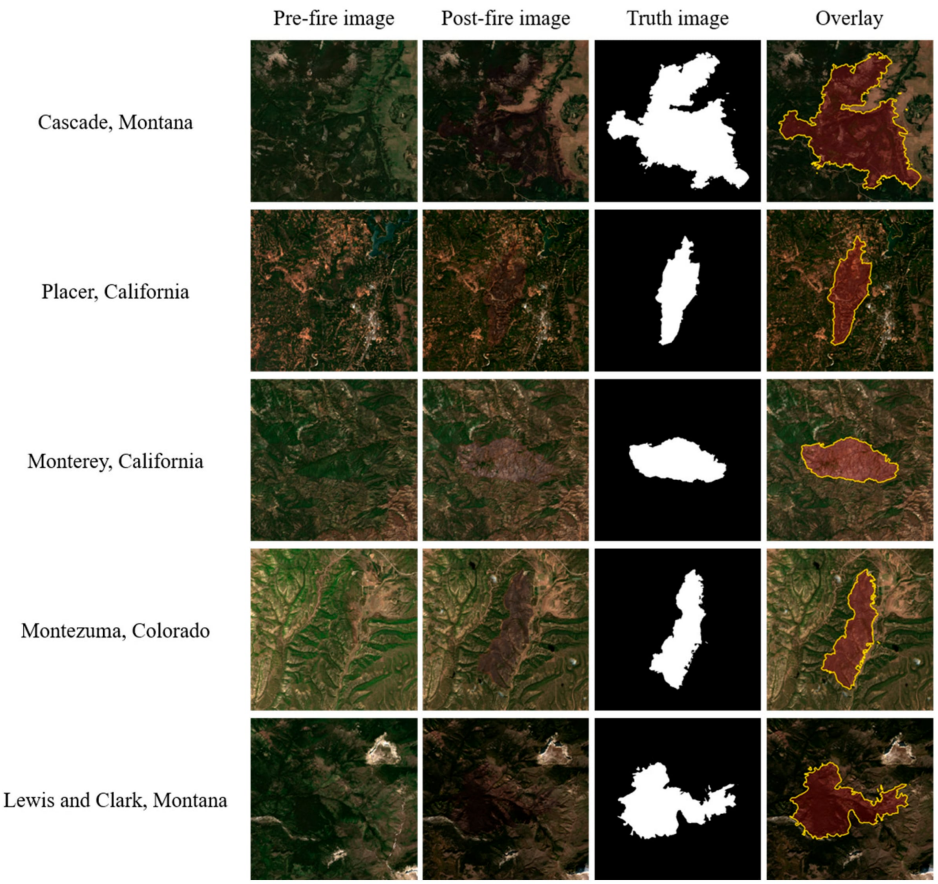

Figure 2. Examples of images and polygons acquired from WFIGS and used as training data.

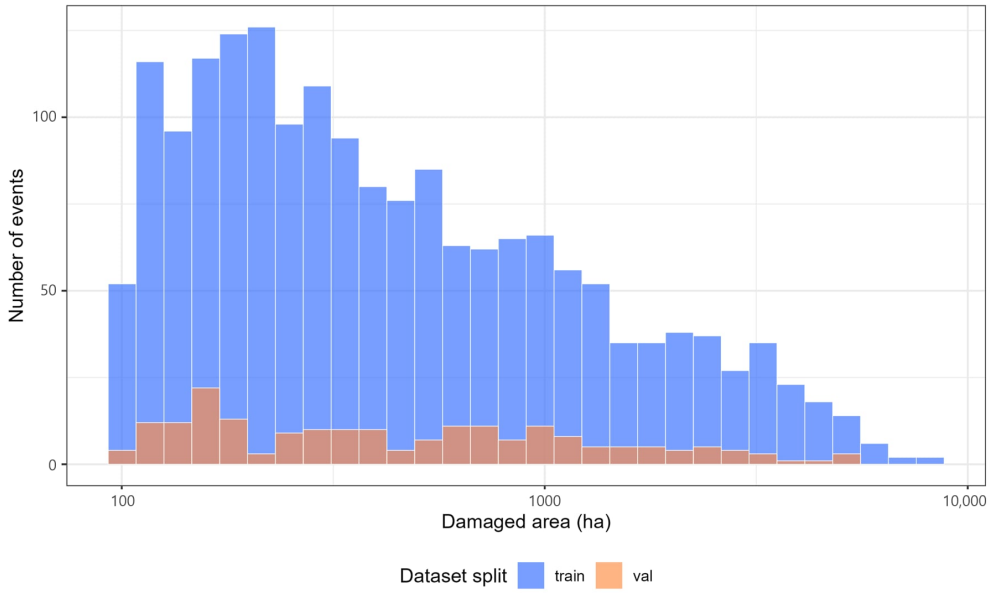

Figure 3. Area distribution of WFIGS data used for model development.

2.2.2. Test and Reference Data

To evaluate the accuracy of the trained models' predictions, forest fire-damaged area boundary data for six forest fire events that occurred in South Korea were obtained. The reference forest fire-damaged area boundaries for each event were generated from high-resolution UAV imagery provided by the National Institute of Forest Science (NIFoS) and were derived from high-resolution UAV imagery [50]. According to the description of the data source, these boundaries were prepared through visual interpretation of the UAV imagery and field visits. These independently prepared reference boundaries were used for the final performance evaluation of the models, whereas the WFIGS perimeters were used only as training labels.

2.2.3. Sentinel-2 Imagery

In this study, Sentinel-2 imagery with a spatial resolution of 10–20 m was used because it includes RedEdge and NIR bands, which are useful for forest fire-damaged area delineation, and its 5-day revisit cycle allows the acquisition of images taken immediately after forest fire events [12,13,19,20]. To improve the accuracy of forest fire damage classification, Level-2A data, for which geometric, orthorectification, radiometric, atmospheric, and terrain corrections had already been applied, were collected through the Sentinel Hub API [51,52]. Sentinel-2 Level-2A imagery was consistently accessed through the Sentinel Hub API for all study sites. During preprocessing, the DN values of the selected bands were divided by 10,000, and the resulting scaled bands were then used to generate the spectral-band composites and vegetation-index inputs for model training and evaluation. To maintain compatibility with the bands used by the Compact Advanced Satellite-500(CAS-500) No. 4, which will be used for future forest fire monitoring operations, B2 (Blue), B3 (Green), B4 (Red), B5 (RedEdge), and B8 (NIR) from the Sentinel-2 imagery were employed in this study. Accordingly, SWIR-based indices such as NBR and dNBR were outside the scope of the present input design. For each fire event, the closest available pre-fire and post-fire Sentinel-2 Level-2A images were selected under the constraints of scene availability, revisit time, and cloud conditions; post-fire images were selected within one month after fire suppression (Table 2). All imagery was resampled to a spatial resolution of 20 m and divided into tiles of 512 × 512 pixels.

Table 2. Pre-fire and post-fire imagery acquisition dates and days after suppression for the study sites.

Study Site	Pre-Fire Imagery Acquisition Date	Post-Fire Imagery Acquisition Date	Days After Suppression
Andong	9 April 2020	29 April 2020	3 days
Bonghwa	4 April 2022	17 April 2022	11 days
Gunwi	9 April 2022	19 April 2022	7 days
Yanggu	7 April 2022	17 April 2022	5 days
Ulgin	9 May 2022	3 June 2022	5 days
Miryang	31 May 2022	18 June 2022	12 days

2.3. Method

The overall workflow of the proposed approach is shown in Figure 4.

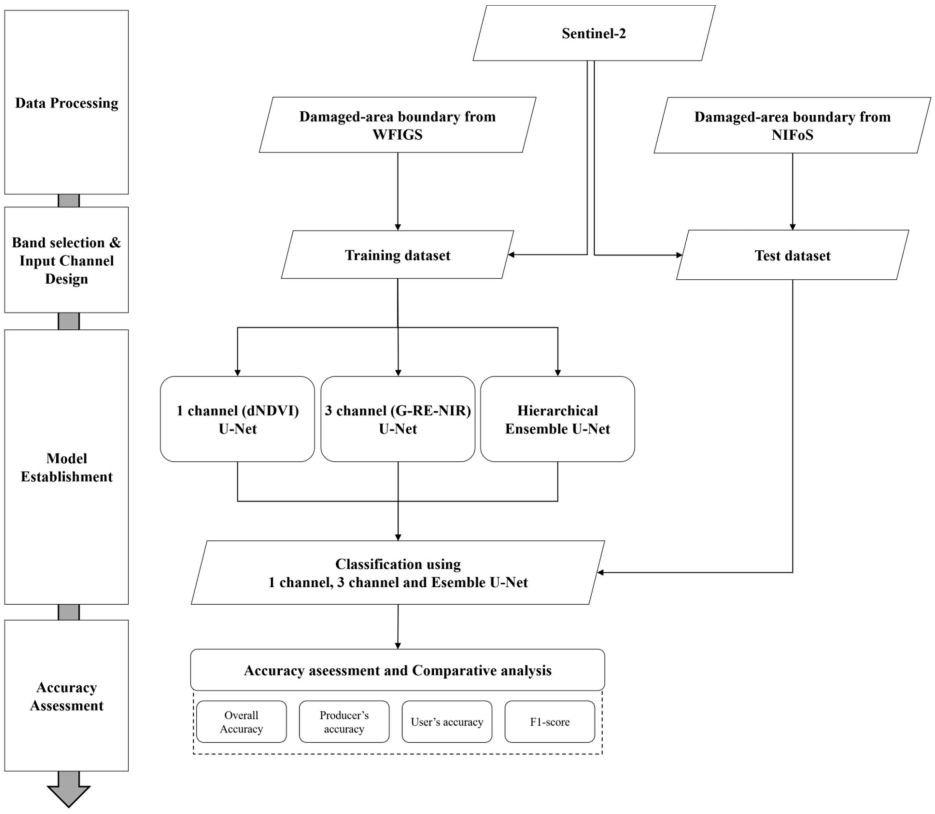

Figure 4. Methodology Flowchart.

2.3.1. Band Selection and Input Channel Design

In this study, input-channel combinations for forest fire damage-boundary delineation were identified through or based on previous studies and an analysis of spectral-value differences [12,15,22–26]. Previous studies indicated that visible-spectrum (Blue, Green, and Red) and vegetation-related (RedEdge and NIR) bands, as well as vegetation indices (the NDVI and dNDVI), have a high potential for delineating forest fire-damage area. A comparison of spectral-value distributions between burned and unburned areas in the training dataset showed that the greatest difference was observed in the NIR band (744.7), followed by the RedEdge (85.8), Green (50.8), Red (43.0), and Blue (12.4) bands. For vegetation indices, the difference was greater for the dNDVI (0.34) than for the NDVI (0.19), indicating that temporal change information was more useful for damage detection (Table 3).

$$NDVI = \frac{NIR - Red}{NIR + Red}$$

$$dNDVI = NDVI_{pre} - NDVI_{post}$$

Table 3. Mean Digital Number (DN) values of and differences between spectral bands and vegetation indices for burned and unburned areas of training data.

Band	Mean Value of Burned Area	Mean Value of Unburned Area	Difference
Blue	383.4	371.0	12.4
Green	519.3	570.1	50.8
Red	550.5	507.5	43.0
RedEdge	866.5	952.3	85.8
NIR	1765.4	2510.1	744.7
NDVI	0.46	0.65	0.19
dNDVI	0.16	−0.18	0.34

Based on the findings of previous studies and the spectral-difference analysis, four three-band combinations (B-G-R, B-G-RE, G-R-NIR, and NIR-RE-G) and two single-index inputs (*NDVI* and *dNDVI*) were selected. These combinations were designed to represent different types of spectral information while maintaining compatibility with CAS-500 imagery for future applications. B-G-R was included as a visible-band baseline, whereas B-G-RE was selected to examine the added contribution of the RedEdge band to a visible-band configuration [53,54]. G-R-NIR was included because the same band combination has been adopted previous forest-fire-damaged area mapping studies [55]. In contrast, NIR-RE-G was newly configured in this study by replacing the Red band in the G-R-NIR combination reported in previous studies with RedEdge, in order to examine whether vegetation-sensitive spectral information could provide additional utility for fire-damage boundary delineation. The relatively large burned–unburned contrasts observed in the Green, RedEdge, and NIR bands (Table 3) also supported the inclusion of this combination (Figure 5). *NDVI* and *dNDVI* were included as representative single-index inputs, with *dNDVI* additionally capturing pre- and post-fire temporal changes [56,57]. Based on these considerations, six input types were selected as candidate spectral configurations for model development.

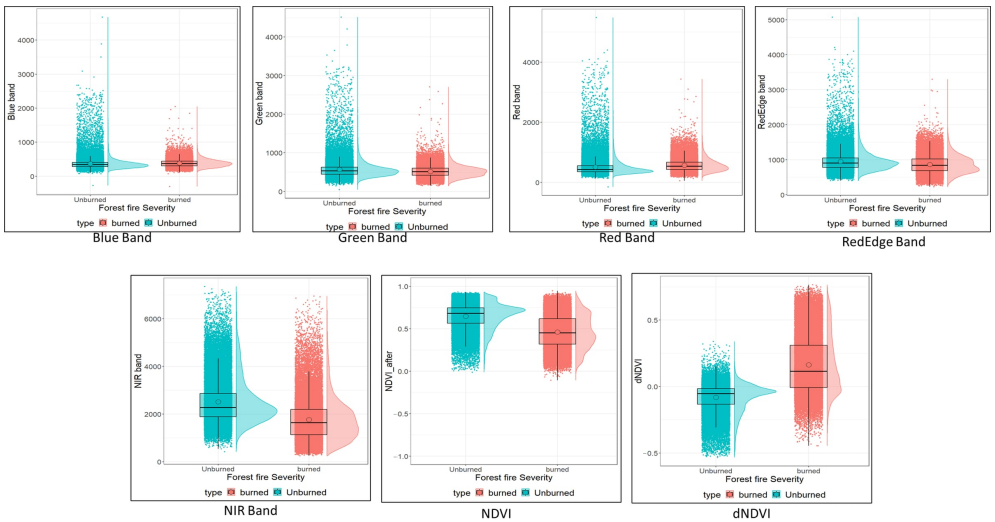

Figure 5. Distribution of spectral values for the Blue, Green, Red, RedEdge, and NIR bands and the index values of the NDVI and dNDVI in burned areas (red) and unburned areas (blue) of training data.

2.3.2. Model Establishment

To compare different model-design strategies rather than to rank all six candidate input types as standalone models, three representative U-Net-based models were constructed and evaluated for forest fire-damaged boundary delineation. The first model used dNDVI as a single-channel input, the second used NIR-RE-G as a three-channel input, and the third was a hierarchical ensemble model integrating all six selected input types. In this design, *dNDVI* and NIR-RE-G were used as representative single-input models, whereas the remaining input combinations were incorporated into the first stage of the ensemble model (Figure 4).

The segmentation models used in this study were implemented using a U-Net-based encoder–decoder architecture with skip connections [43]. The network was configured with an input size of 512 × 512 pixels and four repeated downsampling and upsampling stages. Convolution layers used 3 × 3 kernels with ReLU activation, same padding, and He-normal initialization, and batch normalization was applied before each convolution. Downsampling was performed using 2 × 2 max-pooling, whereas upsampling was implemented using transposed convolution. The final output layer consisted of a 1 × 1 convolution with sigmoid activation to generate a pixel-wise probability map. Because this U-Net structure can accommodate different numbers of input channels by adjusting the first convolutional layer, a one-channel structure was used for the dNDVI model, a three-channel structure was used for the NIR-RE-G model, and a six-channel structure was used in the second stage of the hierarchical ensemble model. The models were compiled with the Adam optimizer and a binary cross-entropy plus Dice loss function and were trained for 100 epochs with 100 steps per epoch and a batch size of 20. Model selection was based on validation loss using a checkpointing strategy.

The hierarchical ensemble model consisted of two sequentially trained stages rather than an end-to-end architecture. In the first stage, six independent U-Net models were trained using the selected spectral configurations (B-G-R, B-G-RE, G-R-NIR, NIR-RE-G, *NDVI*, and *dNDVI*). To reduce same-sample bias between the first and second stages, the probability maps used for second-stage training were generated through a fold-based procedure, in which the first-stage models were trained on learning folds and applied only to held-out folds. The resulting held-out prediction maps, representing pixel-wise probabilities of forest fire damage, were rescaled to 8-bit grayscale images (0–255) and stacked to form a six-channel input dataset. This stacked dataset was then used to train a separate second-stage U-Net model for final boundary delineation.

2.3.3. Accuracy Assessment

Accuracy assessment was conducted for each fire event within an evaluation extent defined from the outermost top, bottom, left, and right positions of the reference fire-damaged boundary. Within this extent, only pixels in forest area at 20 m spatial resolution were included in the assessment, and predicted classification was compared with reference classification on a grid-by-grid basis to construct the error matrix. For each model and each study site, an error matrix was constructed by comparing the predicted classification results with the reference classification data. Based on these error matrices, overall accuracy (OA), producer's accuracy (PA), user's accuracy (UA), *F1-score*, and the kappa coefficient were calculated as follows:

$$OA = \frac{TP + TN}{TP + TN + FP + FN}$$

$$PA = \frac{TP}{TP + FN}$$

$$UA = \frac{TP}{TP + FP}$$

$$F1 - Score = \frac{2 \times PA \times UA}{PA + UA}$$

$$\kappa = \frac{P_o + P_e}{1 - P_e}$$

where TP, TN, FP, and FN denote true positive, true negative, false positive, and false negative, respectively. P_o is the observed agreement, calculated as

$$P_o = \frac{TP + TN}{TP + TN + FP + FN}$$

and P_e is the agreement expected by chance, calculated as

$$P_e = \frac{(TP + FP)(TP + FN) + (FN + TN)(FP + TN)}{(TP + TN + FP + FN)^2}$$

In addition, intersection over union (IoU) was computed as a complementary metric to quantify the spatial overlap between the predicted fire-damaged area and the reference fire-damaged area, as follows:

$$IoU = \frac{Area\ of\ Intersection}{Area\ of\ Union}$$

OA, *PA*, *UA*, kappa coefficient, *F1-score*, and *IoU* were calculated separately for each of the six study sites, and their mean values were used to compare model performance. Based on this evaluation framework, the single-channel dNDVI model, the three-channel NIR-RE-G model, and the hierarchical ensemble model were applied to the six forest fire-damaged sites in South Korea, and their delineation accuracies were compared using the metrics described above.

3. Results

3.1. Model Establishment Results

Figure 6 compares the training and validation learning curves of the *dNDVI*, NIR-RE-G, and hierarchical ensemble models over 100 epochs. Overall, all three models showed progressive decreases in training loss and corresponding increases in training accuracy, indicating that model optimization proceeded stably during the training process. However, the degree of convergence and the gap between training and validation performance differed among the models.

The *dNDVI* model showed the weakest learning behavior among the three models. Although its training loss continuously decreased and its training accuracy gradually increased, the validation loss remained relatively high and fluctuated around a plateau in the later epochs. Likewise, the validation accuracy improved during the early stage of training but then showed limited additional gain. These patterns suggest that the single-index input was less effective in capturing fire-damaged boundary characteristics than the other tested input configurations. In contrast, the NIR-RE-G model showed more favorable convergence patterns than the *dNDVI* model. Its training and validation losses decreased more rapidly during the early epochs, and the validation accuracy reached a consistently higher level. The gap between training and validation performance was still present, but the overall trend indicates that the three-band spectral combination provided more informative input features than the single *dNDVI* index for burned-area boundary delineation. Among the three models, the hierarchical ensemble model showed the most stable and favorable learning behavior. It started with a lower loss and higher accuracy than the other models and maintained these advantages throughout the training process. In particular, both the loss and accuracy curves were relatively flat and stable, with only minor fluctuations in validation performance.

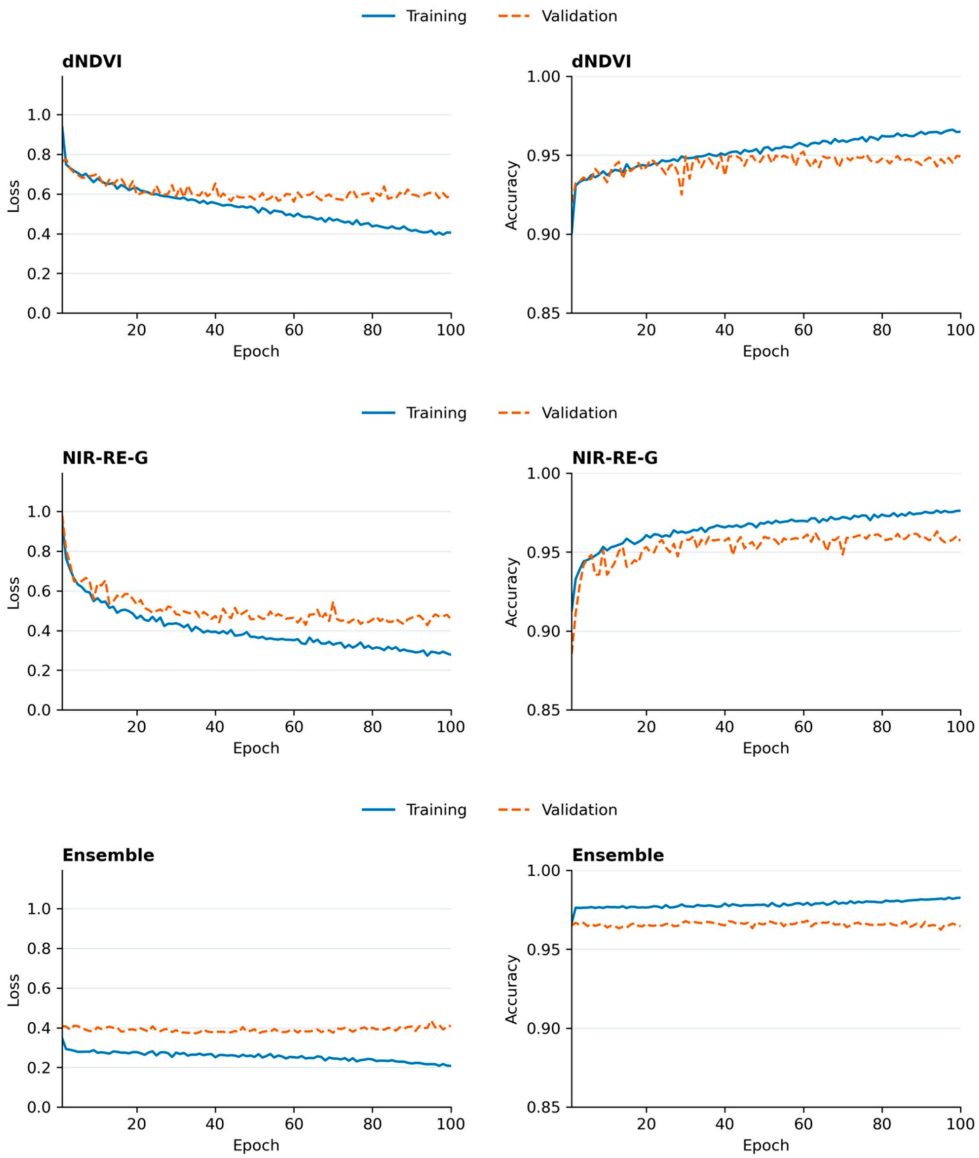

Figure 6. Loss and accuracy curves for the dNDVI, NIR-RE-G, and hierarchical ensemble models over 100 epochs.

3.2. Accuracy Assessment Results

In this study, three U-Net-based segmentation models, a single-channel (*dNDVI*), a three-channel (NIR-RE-G), and an ensemble model, were evaluated using six forest fire-affected areas in South Korea (Figure 7). The overall classification accuracy of each model is summarized in Table 4.

Table 4. Performance metrics for the three tested models, averaged across six fire-damaged study sites in South Korea.

Metrics	Single-Channel dNDVI	Three-Channel NIR-RE-G	Ensemble
Overall accuracy (%)	84.1	82.9	85.7
Producer accuracy (%)	89.0	70.7	92.2
User accuracy (%)	74.2	91.8	75.8
Kappa coefficient	0.67	0.65	0.68
F1-score	0.80	0.77	0.83
IoU	0.68	0.65	0.70

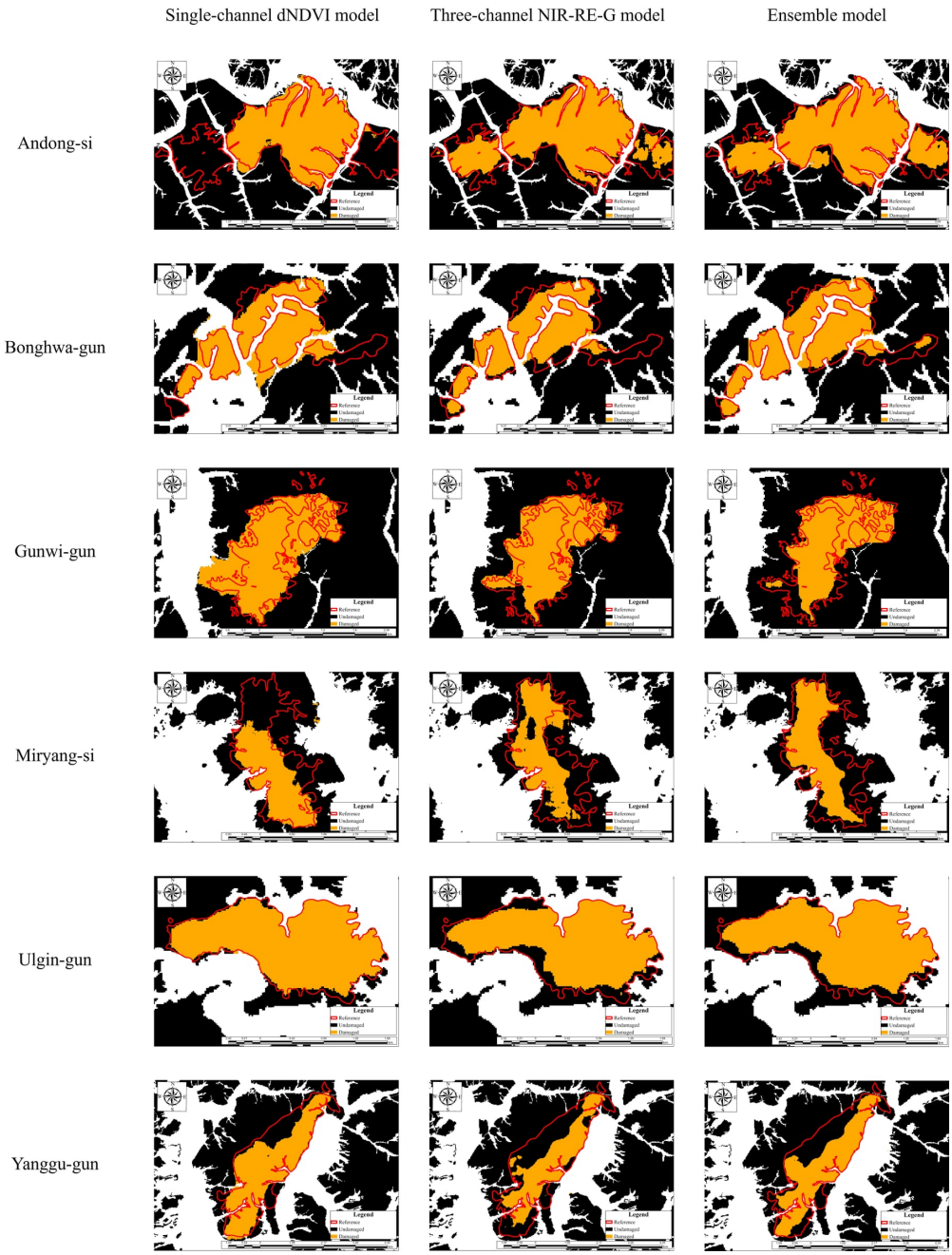

Figure 7. Results of three model's forest fire-damaged area predictions for the six forest fire events in South Korea.

The single-channel *dNDVI* model achieved an overall accuracy of 84.1%, while the producer and user accuracies were 89.0% and 74.2%, with an *F1-score* of 0.80 and an *IoU* of 0.68. The prediction results of this model generally agreed with the reference data in Bonghwa-gun and Ulgin-gun; however, in Andong-si, Miryang-si, and Yanggu-gun, it tended to underestimate the damaged area. These results suggest that single-channel information alone has limitations in accurately capturing certain types of forest fire damage.

The three-channel (NIR-RE-G) model exhibited a slightly lower overall accuracy (82.9%) than the single-channel model. In particular, the producer accuracy was 70.7%, approximately 18 percentage points lower than that of the single-channel model. This indicates that a considerable portion of the actual damaged area was misclassified as undamaged. In contrast, the user accuracy was relatively high, at 91.8%, with an *F1-score* of 0.77 and an *IoU* of 0.65. A detailed analysis suggests that, in Andong-si and Miryang-si, a

relatively large number of false negatives occurred, in which parts of the actual damaged area were classified as undamaged area, reducing the producer accuracy. By contrast, the user accuracy was high because most of the areas identified as damaged corresponded to burned areas.

The ensemble model achieved the highest overall accuracy (85.7%) and exhibited excellent producer accuracy (92.2%), yielding a result similar to the high detection performance of the single-channel model, with an *F1-score* of 0.83 and an *IoU* of 0.70. The user accuracy, 75.8%, was lower than that of the three-channel model, which may be interpreted as a tendency to slightly overestimate damaged areas, although this value remains within an operationally acceptable range. Except for some local misclassifications in Yanggu-gun, the ensemble model accurately delineated damage boundaries in all test areas.

All three models showed undetected areas in the southeastern part of Miryang-si and the northwestern part of Yanggu-gun. Visual comparison with the Sentinel-2 imagery indicated that some of these areas, although included within the reference provided by NIFoS, did not exhibit clearly charred surface features and instead retained a relatively green appearance. This pattern suggests that damage associated with relatively low-intensity surface fires may be more difficult to delineate using optical satellite imagery alone.

4. Discussion

Using U-Net-based forest fire damage boundary delineation models with different input-data compositions, this study evaluated the applicability of models trained on an external fire-perimeter dataset to forest fire-damaged areas in South Korea and examined the influence of input configuration on delineation performance. Comparison of the single-channel, three-channel, and hierarchical ensemble models showed that delineation performance was influenced by how spectral inputs were structured and integrated.

The relative performance of the three models suggests that the two non-ensemble models were useful for forest fire damage delineation, although they were less effective than the hierarchical ensemble model in representing the full complexity of forest fire-affected areas. The single-channel *dNDVI* model was effective for detecting overall fire-affected areas because of its sensitivity to vegetation change, although its tendency to delineate damaged boundaries more narrowly than the reference extent suggests that a single index alone may be less effective in representing subtle damage patterns.

Similarly, the three-channel NIR-RE-G model showed relatively reliable identification of damaged areas, but its lower producer accuracy indicates that a single spectral combination was less effective in capturing the full spatial extent of heterogeneous or transitional fire-damaged areas. Although this configuration was supported by relatively large burned–unburned contrasts at the band level, these contrasts did not translate directly into the highest segmentation performance, suggesting that it was effective for identifying spectrally distinct damaged pixels but not for delineating their full extent. This interpretation is consistent with previous studies showing that spectral indices and conventional machine-learning approaches can provide useful post-fire mapping results, although their performance may vary depending on the representativeness of the selected variables or feature sets [20,32].

By contrast, the hierarchical ensemble model showed the highest average delineation performance among the three models, particularly in terms of overall accuracy, producer accuracy, and *F1-score*. This suggests that integrating predictions derived from different spectral combinations and vegetation indices may overcome the limitations of individual inputs and represent fire-damaged areas more comprehensively. These findings are consistent with previous studies showing that integrating multiple spectral indices or heterogeneous spectral information can improve burned-area mapping performance [45,46], as well as recent deep-learning studies reporting strong burned-area segmentation performance using

Sentinel-2 imagery [33,41,44]. However, direct comparisons of reported accuracies should be interpreted cautiously because of differences in study areas, topographic complexity, reference-data quality, and validation design. Previous studies in South Korea also reported high accuracies for burned-area detection or severity mapping [14,20,34]. For example, Lee et al. [34] reported that U-Net achieved the highest accuracy among the tested models, whereas Lee et al. [20] demonstrated high classification performance using SVM-based approaches. Nevertheless, these studies primarily demonstrated model performance within their respective study areas and data conditions, whereas the present study evaluated the applicability of models trained on external forest-fire datasets to fire-damaged areas in South Korea. The results suggest that externally trained models may have practical utility for case-based boundary delineation across multiple forest-fire sites in South Korea.

At the same time, the misclassification of surface-fire areas in all three models highlights an inherent limitation of optical-satellite-based forest fire damage detection. These areas were associated with relatively weak changes in vegetation reflectance, suggesting that low-intensity fire damage cannot always be distinguished reliably using spectral information alone. Because most of the study sites were in mountainous terrain, topographic effects such as slope aspect and terrain-induced shadows may also have contributed to local omission or misclassification patterns. In addition, the differences in accuracy and loss between the training and validation curves suggest potential limitations in generalization performance, which may reduce prediction reliability near the boundaries of fire-damaged areas. Although detection of core damaged areas appeared relatively stable, increased uncertainty near the boundaries may have contributed to the overestimation observed in some regions. From an operational perspective, such overestimation may be acceptable in situations where omission of damaged areas poses greater challenges for post-fire management. Therefore, future studies should consider improving model generalization and incorporating DEM-based terrain variables or topographic correction to address boundary uncertainty and terrain-related classification errors.

While the proposed model showed promising performance for the six tested fire events in South Korea, several limitations should be noted. First, the temporal intervals between pre-fire and post-fire images were not identical across all cases because image selection was constrained by Sentinel-2 scene availability, revisit timing, and cloud conditions. As a result, some case-specific *dNDVI* responses may have been partly influenced by seasonal vegetation changes during the spring green-up period, and this uncertainty should be considered when interpreting the results. In addition, although Sentinel-2 Level-2A imagery was consistently accessed through Sentinel Hub, the potential influence of product-processing differences could not be fully excluded for the 2020 Andong case and should therefore be considered when interpreting the results. Second, direct quantitative comparison with existing burned-area products was not conducted because most currently available products are designed for regional burned-area monitoring at coarser spatial resolutions and are therefore not directly comparable to the 20 m boundary delineation results presented in this study. Third, broader quantitative validation across additional years and regions was constrained by the limited availability of field-validated reference boundaries of comparable quality. Accordingly, the present results should be interpreted as evidence of the model's applicability to the six tested cases rather than as a comprehensive validation across all fire conditions in South Korea. Further comparison with operational burned-area products and broader validation across additional years, sites, and fire regimes will be necessary in future studies.

5. Conclusions

In this study, models were trained on WFIGS fire-perimeter data from the United States, and their prediction performance was evaluated for six large forest fire-affected areas in South Korea. Rather than assuming direct transferability across all forest-fire environments, this study examined whether externally trained models could support case-based boundary delineation in South Korea and whether a hierarchical structure integrating independent models with different spectral combinations and vegetation indices could improve delineation performance.

The results of this study suggest that models trained on external forest fire data can help address limitations arising from insufficient regional training data. In particular, the hierarchical ensemble model achieved higher delineation accuracy than the single-input models by integrating different spectral inputs to better represent the spectral and spatial heterogeneity of forest fire-affected areas. These findings confirm the importance of input-data configuration and suggest that the proposed ensemble approach may serve as a useful reference for future forest fire damage detection models. Moreover, the application of the model trained on WFIGS fire-perimeter data to forest fire-damaged areas in South Korea indicates its potential transferability to other regions with similar environmental and vegetation characteristics, although further validation is required.

From a practical perspective, the findings of this study are meaningful in that they demonstrate the applicability of high-resolution satellite imagery and deep-learning techniques to environmental disaster management. In addition, the CAS-500 satellite, which has the same band specifications as Sentinel-2 but an improved spatial resolution of 5 m, is expected to enable continuous and stable forest fire damage detection using the proposed model after its launch. Through this approach, more proactive disaster response may become possible, enhancing sustainable forest management and climate resilience.

Despite the high accuracy achieved in delineating large forest fire-damaged areas, several limitations remain. In areas adjacent to urban regions or where vegetation had already entered the recovery stage, model accuracy was lower, indicating a need for improved preprocessing techniques and more diverse training data. In addition, because model evaluation focused on forest fires covering over 100 ha, future studies should include smaller fires and consider differences in damage size and intensity to better define the model's applicability. The integration of additional environmental and topographic variables, such as soil characteristics, multi-temporal vegetation indices, and detailed topographic information, may further improve model performance by better representing spatial variability within fire-damaged areas.

Author Contributions: Conceptualization, G.J., C.W. and J.P.; methodology, G.J., M.L. and J.P.; software, G.J., S.H. and M.L.; validation, G.J., M.L., N.P., B.C. and B.K.; formal analysis, G.J. and S.H.; investigation, G.J., S.H., M.L. and B.K.; resources, G.J., S.H. and C.W.; data curation, G.J., S.H., N.P., B.C. and C.W.; writing—original draft preparation, G.J.; writing—review and editing, Y.K. and J.P.; visualization, G.J.; supervision, C.W., Y.K. and J.P.; project administration, Y.K. and J.P.; funding acquisition, C.W. and J.P. All authors have read and agreed to the published version of the manuscript.

Funding: This study was carried out with the support of 'R&D Program for Forest Science Technology (RS-2019-KF000705)' provided by Korea Forest Service (Korea Forestry Promotion Institute) and 'NIFoS Project (FM0103-2021-02)' provided by National Institute of Forest Science.

Data Availability Statement: The data presented in this study are available on request from the corresponding author. The data are not publicly available due to institutional distribution restrictions.

Conflicts of Interest: The authors declare no conflicts of interest.

Abbreviations

The following abbreviations are used in this manuscript:

API	Application Programming Interface
CART	Classification and Regression Trees
CAS-500	Compact Advanced Satellite-500
dNDVI	differenced NDVI
DL	Deep Learning
IRWIN	Integrated Reporting of Wildland Fire Information
ISODATA	Iterative Self-Organizing Data Analysis Technique
ML	Machine Learning
MODIS	Moderate Resolution Imaging Spectroradiometer
NBR	Normalized Burn Ratio
NDVI	Normalized Difference Vegetation Index
NIFoS	National Institute of Forest Science
SAR	Synthetic Aperture Radar
SVM	Support Vector Machine
UAV	Unmanned Aerial Vehicle
U-Net	U-shaped Network
USDA	United States Department of Agriculture
WFIGS	Wildland Fire Interagency Geospatial Services
R	Red
G	Green
B	Blue
RE	RedEdge
NIR	Near-Infrared

References

1. Boer, M.M.; Resco de Dios, V.; Bradstock, R.A. Unprecedented burn area of Australian mega forest fires. *Nat. Clim. Change* **2020**, *10*, 171–172. [CrossRef]
2. Bowman, D.; Moreira-Muñoz, A.; Kolden, C.A.; Chávez, R.O.; Muñoz, A.A.; Salinas, F.; González-Reyes, Á.; Rocco, R.; de la Barrera, F.; Williamson, G.J.; et al. Human-environmental drivers and impacts of the globally extreme 2017 Chilean fires. *Ambio* **2019**, *48*, 350–362. [CrossRef] [PubMed]
3. Giglio, L.; Randerson, J.T.; van der Werf, G.R. Analysis of daily, monthly, and annual burned area using the fourth-generation global fire emissions database (GFED4). *J. Geophys. Res. Biogeosci.* **2013**, *118*, 317–328. [CrossRef]
4. Rhoades, C.; Entwistle, D.; Butler, D. The influence of wildfire extent and severity on streamwater chemistry, sediment and temperature following the Hayman Fire, ColoradoA. *Int. J. Wildland Fire* **2011**, *20*, 430–442. [CrossRef]
5. Lewis, S.A.; Robichaud, P.R.; Archer, V.A.; Hudak, A.T.; Eitel, J.U.H.; Strand, E.K. Informing Sustainable Forest Management: Remote Sensing Strategies for Assessing Soil Disturbance after Wildfire and Salvage Logging. *Forests* **2023**, *14*, 2218. [CrossRef]
6. Noske, P.J.; Nyman, P.; Lane, P.N.J.; Rengers, F.K.; Sheridan, G.J. Changes in soil erosion caused by wildfire: A conceptual biogeographic model. *Geomorphology* **2024**, *459*, 109272. [CrossRef]
7. Pezzatti, G.B.; De Angelis, A.; Bekar, İ.; Ricotta, C.; Bajocco, S.; Conedera, M. Complementing daily fire-danger assessment using a novel metric based on burnt area ranking. *Agric. For. Meteorol.* **2020**, *295*, 108172. [CrossRef]
8. Zhang, S.; Bai, M.; Wang, X.; Peng, X.; Chen, A.; Peng, P. Remote sensing technology for rapid extraction of burned areas and ecosystem environmental assessment. *PeerJ* **2023**, *11*, e14557. [CrossRef] [PubMed]
9. Lindenmayer, D.B.; Noss, R.F. Salvage Logging, Ecosystem Processes, and Biodiversity Conservation. *Conserv. Biol.* **2006**, *20*, 949–958. [CrossRef] [PubMed]
10. Jain, P.; Coogan, S.C.P.; Subramanian, S.G.; Crowley, M.; Taylor, S.; Flannigan, M.D. A review of machine learning applications in wildfire science and management. *Environ. Rev.* **2020**, *28*, 478–505. [CrossRef]
11. Pan, Y.; Birdsey, R.A.; Fang, J.; Houghton, R.; Kauppi, P.E.; Kurz, W.A.; Phillips, O.L.; Shvidenko, A.; Lewis, S.L.; Canadell, J.G.; et al. A Large and Persistent Carbon Sink in the World's Forests. *Science* **2011**, *333*, 988–993. [CrossRef] [PubMed]
12. Roteta, E.; Bastarrika, A.; Padilla, M.; Storm, T.; Chuvieco, E. Development of a Sentinel-2 burned area algorithm: Generation of a small fire database for sub-Saharan Africa. *Remote Sens. Environ.* **2019**, *222*, 1–17. [CrossRef]
13. Roy, D.P.; Huang, H.; Boschetti, L.; Giglio, L.; Yan, L.; Zhang, H.H.; Li, Z. Landsat-8 and Sentinel-2 burned area mapping—A combined sensor multi-temporal change detection approach. *Remote Sens. Environ.* **2019**, *231*, 111254. [CrossRef]
14. Sim, S.; Kim, W.; Lee, J.; Kang, Y.; Im, J.; Kwon, C.; Kim, S. Wildfire Severity Mapping Using Sentinel Satellite Data Based on Machine Learning Approaches. *Korean J. Remote Sens.* **2020**, *36*, 1109–1123. [CrossRef]

15. Kontoes, C.C.; Poilvé, H.; Florsch, G.; Keramitsoglou, I.; Paralikidis, S. A comparative analysis of a fixed thresholding vs. a classification tree approach for operational burn scar detection and mapping. *Int. J. Appl. Earth Obs. Geoinf.* **2009**, *11*, 299–316. [CrossRef]
16. Chuvieco, E.; Mouillot, F.; van der Werf, G.R.; San Miguel, J.; Tanase, M.; Koutsias, N.; García, M.; Yebra, M.; Padilla, M.; Gitas, I.; et al. Historical background and current developments for mapping burned area from satellite Earth observation. *Remote Sens. Environ.* **2019**, *225*, 45–64. [CrossRef]
17. Giglio, L.; Boschetti, L.; Roy, D.P.; Humber, M.L.; Justice, C.O. The Collection 6 MODIS burned area mapping algorithm and product. *Remote Sens. Environ.* **2018**, *217*, 72–85. [CrossRef] [PubMed]
18. Moreno-Ruiz, J.A.; García-Lázaro, J.R.; Arbelo, M.; Cantón-Garbín, M. MODIS Sensor Capability to Burned Area Mapping—Assessment of Performance and Improvements Provided by the Latest Standard Products in Boreal Regions. *Sensors* **2020**, *20*, 5423. [CrossRef] [PubMed]
19. Wang, H.; Zhang, X.; Xue, W.; Qin, C.; Wu, Y.; Wang, S.; Qiu, P. Evaluation of forest fire damage based on Sentinel-2 images. In Proceedings of the International Conference on Environmental Remote Sensing and Big Data (ERSBD), Wuhan, China, 29–31 October 2021.
20. Lee, S.-H.; Lee, M.-H.; Kang, T.-H.; Cho, H.-R.; Yun, H.-S.; Lee, S.-J. Comparative Analysis of dNBR, dNDVI, SVM Kernels, and ISODATA for Wildfire-Burned Area Mapping Using Sentinel-2 Imagery. *Remote Sens.* **2025**, *17*, 2196. [CrossRef]
21. Chu, T.; Guo, X. Remote Sensing Techniques in Monitoring Post-Fire Effects and Patterns of Forest Recovery in Boreal Forest Regions: A Review. *Remote Sens.* **2014**, *6*, 470–520. [CrossRef]
22. Kasischke, E.S.; French, N.H.F. Locating and estimating the areal extent of wildfires in alaskan boreal forests using multiple-season AVHRR NDVI composite data. *Remote Sens. Environ.* **1995**, *51*, 263–275. [CrossRef]
23. Loboda, T.; O'Neal, K.J.; Csiszar, I. Regionally adaptable dNBR-based algorithm for burned area mapping from MODIS data. *Remote Sens. Environ.* **2007**, *109*, 429–442. [CrossRef]
24. Quintano, C.; Fernández-Manso, A.; Fernández-Manso, O. Combination of Landsat and Sentinel-2 MSI data for initial assessing of burn severity. *Int. J. Appl. Earth Obs. Geoinf.* **2018**, *64*, 221–225. [CrossRef]
25. Lentile, L.B.; Holden, Z.A.; Smith, A.M.S.; Falkowski, M.J.; Hudak, A.T.; Morgan, P.; Lewis, S.A.; Gessler, P.E.; Benson, N.C. Remote sensing techniques to assess active fire characteristics and post-fire effects. *Int. J. Wildland Fire* **2006**, *15*, 319–345. [CrossRef]
26. Tiengo, R.; Merino-De-Miguel, S.; Uchôa, J.; Guiomar, N.; Gil, A. Burned Areas Mapping Using Sentinel-2 Data and a Rao's Q Index-Based Change Detection Approach: A Case Study in Three Mediterranean Islands' Wildfires (2019–2022). *Remote Sens.* **2025**, *17*, 830. [CrossRef]
27. Boschetti, L.; Roy, D.P.; Giglio, L.; Huang, H.; Zubkova, M.; Humber, M.L. Global validation of the collection 6 MODIS burned area product. *Remote Sens. Environ.* **2019**, *235*, 111490. [CrossRef] [PubMed]
28. Sismanis, M.; Chadoulis, R.; Manakos, I.; Drosou, A. An Unsupervised Burned Area Mapping Approach Using Sentinel-2 Images. *Land* **2023**, *12*, 379. [CrossRef]
29. Lee, S.; Lee, Y. Detection of Wildfire-Damaged Areas Using Kompsat-3 Image: A Case of the 2019 Unbong Mountain Fire in Busan, South Korea. *Korean J. Remote Sens.* **2020**, *36*, 29–39. [CrossRef]
30. Gündüz, H.İ.; Torun, A.T.; Gezgin, C. Post-Fire Burned Area Detection Using Machine Learning and Burn Severity Classification with Spectral Indices in İzmir: A SHAP-Driven XAI Approach. *Fire* **2025**, *8*, 121. [CrossRef]
31. Singh, H.; Ang, L.-M.; Srivastava, S.K. Active wildfire detection via satellite imagery and machine learning: An empirical investigation of Australian wildfires. *Nat. Hazards* **2025**, *121*, 9777–9800. [CrossRef]
32. Bar, S.; Parida, B.R.; Pandey, A.C. Landsat-8 and Sentinel-2 based Forest fire burn area mapping using machine learning algorithms on GEE cloud platform over Uttarakhand, Western Himalaya. *Remote Sens. Appl. Soc. Environ.* **2020**, *18*, 100324. [CrossRef]
33. Atasever, Ü.H.; Tercan, E. Deep learning-based burned forest areas mapping via Sentinel-2 imagery: A comparative study. *Environ. Sci. Pollut. Res.* **2024**, *31*, 5304–5318. [CrossRef] [PubMed]
34. Lee, C.; Park, S.; Kim, T.; Liu, S.; Md Reba, M.N.; Oh, J.; Han, Y. Machine Learning-Based Forest Burned Area Detection with Various Input Variables: A Case Study of South Korea. *Appl. Sci.* **2022**, *12*, 10077. [CrossRef]
35. Sui, T.; Huang, Q.; Wu, M.; Wu, M.; Zhang, Z. BiAU-Net: Wildfire burnt area mapping using bi-temporal Sentinel-2 imagery and U-Net with attention mechanism. *Int. J. Appl. Earth Obs. Geoinf.* **2024**, *132*, 104034. [CrossRef]
36. Yilmaz, E.O.; Kavzoglu, T. Burned Area Detection with Sentinel-2A Data: Using Deep Learning Techniques with eXplainable Artificial Intelligence. *ISPRS Ann. Photogramm. Remote Sens. Spat. Inf. Sci.* **2024**, *X-5-2024*, 251–257. [CrossRef]
37. Lee, D.; Son, S.; Bae, J.; Park, S.; Seo, J.; Seo, D.; Lee, Y.; Kim, J. Single-Temporal Sentinel-2 for Analyzing Burned Area Detection Methods: A Study of 14 Cases in Republic of Korea Considering Land Cover. *Remote Sens.* **2024**, *16*, 884. [CrossRef]
38. French, N.H.F.; de Groot, W.J.; Jenkins, L.K.; Rogers, B.M.; Alvarado, E.; Amiro, B.; de Jong, B.; Goetz, S.; Hoy, E.; Hyer, E.; et al. Model comparisons for estimating carbon emissions from North American wildland fire. *J. Geophys. Res. Biogeosci.* **2011**, *116*, G00K05. [CrossRef]

39. Zhu, X.X.; Tuia, D.; Mou, L.; Xia, G.S.; Zhang, L.; Xu, F.; Fraundorfer, F. Deep Learning in Remote Sensing: A Comprehensive Review and List of Resources. *IEEE Geosci. Remote Sens. Mag.* **2017**, *5*, 8–36. [CrossRef]
40. Ghali, R.; Akhloufi, M.A. Deep Learning Approaches for Wildland Fires Using Satellite Remote Sensing Data: Detection, Mapping, and Prediction. *Fire* **2023**, *6*, 192. [CrossRef]
41. Al-Dabbagh, A.M.; Ilyas, M. Uni-temporal Sentinel-2 imagery for wildfire detection using deep learning semantic segmentation models. *Geomat. Nat. Hazards Risk* **2023**, *14*, 2196370. [CrossRef]
42. Knopp, L.; Wieland, M.; Rättich, M.; Martinis, S. A Deep Learning Approach for Burned Area Segmentation with Sentinel-2 Data. *Remote Sens.* **2020**, *12*, 2422. [CrossRef]
43. Ronneberger, O.; Fischer, P.; Brox, T. U-Net: Convolutional Networks for Biomedical Image Segmentation. In *Proceedings of the Medical Image Computing and Computer-Assisted Intervention—MICCAI 2015, Munich, Germany, 5–9 October 2015*; Springer: Cham, Switzerland, 2015; pp. 234–241.
44. Zhang, Q.; Ge, L.; Zhang, R.; Metternicht, G.I.; Du, Z.; Kuang, J.; Xu, M. Deep-learning-based burned area mapping using the synergy of Sentinel-1&2 data. *Remote Sens. Environ.* **2021**, *264*, 112575. [CrossRef]
45. Ba, R.; Song, W.; Li, X.; Xie, Z.; Lo, S. Integration of Multiple Spectral Indices and a Neural Network for Burned Area Mapping Based on MODIS Data. *Remote Sens.* **2019**, *11*, 326. [CrossRef]
46. Smiraglia, D.; Filipponi, F.; Mandrone, S.; Tornato, A.; Taramelli, A. Agreement Index for Burned Area Mapping: Integration of Multiple Spectral Indices Using Sentinel-2 Satellite Images. *Remote Sens.* **2020**, *12*, 1862. [CrossRef]
47. Seydi, S.T.; Hasanlou, M.; Chanussot, J. Burnt-Net: Wildfire burned area mapping with single post-fire Sentinel-2 data and deep learning morphological neural network. *Ecol. Indic.* **2022**, *140*, 108999. [CrossRef]
48. Hu, X.; Zhang, P.; Ban, Y. Large-scale burn severity mapping in multispectral imagery using deep semantic segmentation models. *ISPRS J. Photogramm. Remote Sens.* **2023**, *196*, 228–240. [CrossRef]
49. National Interagency Fire Center. WFIGS Interagency Fire Perimeters. 2024. Available online: https://data-nifc.opendata.arcgis.com/datasets/nifc::wfigs-interagency-fire-perimeters/about (accessed on 9 July 2024).
50. National Institute of Forest Science. *Forest Fire-Damaged Area Boundaries*; NIFoS: Seoul, Republic of Korea, 2023.
51. Copernicus Data Space Ecosystem. Sentinel-2 L2A API. Available online: https://documentation.dataspace.copernicus.eu/APIs/SentinelHub/Data/S2L2A.html?utm_source=chatgpt.com (accessed on 9 July 2024).
52. Copernicus Sentinel-2 (processed by ESA). MSI Level-2A BOA Reflectance Product. 2021. Available online: https://sentinels.copernicus.eu/web/sentinel/sentinel-data-access/sentinel-products/sentinel-2-data-products/collection-0-level-2a (accessed on 14 July 2024).
53. Delegido, J.; Verrelst, J.; Alonso, L.; Moreno, J. Evaluation of Sentinel-2 Red-Edge Bands for Empirical Estimation of Green LAI and Chlorophyll Content. *Sensors* **2011**, *11*, 7063–7081. [CrossRef] [PubMed]
54. Fernández-Manso, A.; Fernández-Manso, O.; Quintano, C. SENTINEL-2A red-edge spectral indices suitability for discriminating burn severity. *Int. J. Appl. Earth Obs. Geoinf.* **2016**, *50*, 170–175. [CrossRef]
55. Kilic, A.; Kulavuz, B.; Bakirman, T.; Bayram, B. Comparison of Two Deep Learning Models to Determine Burned Forest Areas from Sentinel-2 Imagery. *Balt. J. Mod. Comput.* **2024**, *12*, 443–453. [CrossRef]
56. Teodoro, A.; Amaral, A. A Statistical and Spatial Analysis of Portuguese Forest Fires in Summer 2016 Considering Landsat 8 and Sentinel 2A Data. *Environments* **2019**, *6*, 36. [CrossRef]
57. Tran, B.; Tanase, M.; Bennett, L.; Aponte, C. Evaluation of Spectral Indices for Assessing Fire Severity in Australian Temperate Forests. *Remote Sens.* **2018**, *10*, 1680. [CrossRef]

Disclaimer/Publisher's Note: The statements, opinions and data contained in all publications are solely those of the individual author(s) and contributor(s) and not of MDPI and/or the editor(s). MDPI and/or the editor(s) disclaim responsibility for any injury to people or property resulting from any ideas, methods, instructions or products referred to in the content.